Orbital angular momentum in radio—a system study

Siavoush M. Mohammadi, Lars K. S. Daldorff, Jan E. S. Bergman, Roger L. Karlsson, *Member, IEEE,* Bo Thidé, Kamyar Forozesh, *Student Member, IEEE* and Tobia D. Carozzi

***Abstract*—Recent discoveries concerning rotating (helical) phase fronts and orbital angular momentum (OAM) of laser beams are applied to radio frequencies and comprehensive simulations of a radio OAM system are performed. We find that with the use of vector field sensing electric and magnetic triaxial antennas, it is possible to unambiguously estimate the OAM in radio beams by local measurements at a single point, provided ideal (noiseless) conditions and that the beam axis is known. Furthermore, we show that conventional antenna pattern optimization methods can be applied to OAM generating circular arrays to enhance their directivity.**

***Index Terms*—orbital angular momentum, radio orbital angular momentum, microwave orbital angular momentum, directivity optimization, rotating phase fronts.**

I. Introduction

As described in the standard electrodynamics literature, an electromagnetic (EM) system will not only radiate energy (linear momentum) but also angular momentum (AM) into the far zone [1], [2]. Already during the early 20th century, predictions of how the polarization of light, *i.e.*, the spin part of the angular momentum (SAM), could transfer angular momentum to a mechanical system were made. In 1935, Beth [3] demonstrated experimentally that this was indeed possible. However, it is only recently that the orbital part of the electromagnetic angular momentum (OAM) has found practical use [4], [5]. Hitherto, the applications have mostly been within the optical regime, but the basic physical properties of the EM fields can be translated from optics to radio; in 2007 the first radio OAM simulations were performed [6]. In the present paper, we make a comprehensive system simulation of OAM carried by radio beams generated by a circular antenna array. It should be emphasized that it is sufficient, but not necessary, to use antenna arrays to generate OAM. Methods using optical elements as in the optical experiments will also give rise to OAM-carrying radio beams [7].

The system simulation will be performed in two steps. First, we address issues concerning the generation and directivity of OAM radio beams, while the second part of the paper concerns the measurement of OAM at radio frequencies.

It is important to remember that angular momentum (AM) behaves similarly to other conserved electromagnetic quantities such as energy and linear momentum. The AM modes, and hence also the OAM modes, are therefore carried by radio beams just as other conserved electromagnetic quantities are.

In this paper, the EM field data are always referring to the three–dimensional (3D), electric and magnetic vector fields, with complete phase information.

Siavoush M. Mohammadi, Jan E. S. Bergman and Bo Thidé are with the Swedish Institute of Space Physics, Uppsala, P. O. Box 537, SE-751 21 Uppsala, Sweden e-mail: simo@irfu.se

Lars K. S. Daldorff, Roger Karlsson and Kamyar Forozesh are with the Department of Physics and Astronomy, Uppsala University, P. O. Box 516, SE-751 20 Uppsala, Sweden

Roger Karlsson is with the Space Research Institute, Austrian Academy of Sciences, Schmiedlstrasse 6, A-8042 Graz, Austria

Tobia D. Carozzi is with the Department of Physics and Astronomy, University of Glasgow, Glasgow G12 8QQ Scotland, United Kingdom

Manuscript received ..., ...; revised ....., ...

II. Theoretical background

The angular momentum (of a spectral component) of the electromagnetic field,

$$\mathbf{J} = \int \varepsilon_0 \mathbf{r} \times \mathrm{Re}\{\mathbf{E} \times \mathbf{B}^*\}\,\mathrm{d}V \tag{1}$$

can in a beam geometry be decomposed into a polarization dependent intrinsic rotation (SAM) and an extrinsic rotation (OAM) [8]. This decomposition of angular momentum is often referred to as the Humblet decomposition [9]. Polarization is the classical manifestation of the quantum mechanical concept spin and we will refer to the intrinsic, polarization dependent, rotation as spin angular momentum (SAM) with mode number denoted s. The extrinsic rotation is referred to as orbital angular momentum (OAM) with mode number l. The angular momentum is the composition of OAM and SAM such that the AM mode number $j = l + s$. The angular momentum mode number can be explicitly calculated from the formula [1]

$$j = \frac{\omega J_z}{\frac{\varepsilon_0}{2}\int(|\mathbf{E}|^2 + c^2|\mathbf{B}|^2)\mathrm{d}V}, \tag{2}$$

The general characteristic of an OAM beam is that the fields have rotating *phase fronts* [10]; see Fig. 1. This contrasts with polarized beams, which have rotating electric *field vectors*. Generally, the polarization dependent part can be found by measuring the 3D generalized Stokes parameter $\mathbf{V}$ [11], [12], [13], whereas the OAM part necessarily needs to be calculated from $\mathbf{J}$ explicitly, either trough the Humblet decomposition or by taking the difference between the "spin" (proportional to $\mathbf{V}$) and the angular momentum $\mathbf{J}$.

III. Antenna simulation setup

The language of electromagnetic orbital angular momentum is borrowed from both classical and quantum mechanics. While it is not common to describe antennas in quantum language, the field characteristics of photon laser experiments [5] can be reproduced in the radio regime. The OAM carrying fields can be generated in a simple way by a phased circular antenna array, where the N array elements, distributed equidistantly around the perimeter of the circle, are phased such that the phase difference between each element is $\delta\phi = 2\pi l/N$, and l is the desired OAM state [6]. The array defines the xy plane with the z axis normal to this plane; see Fig. 2. In

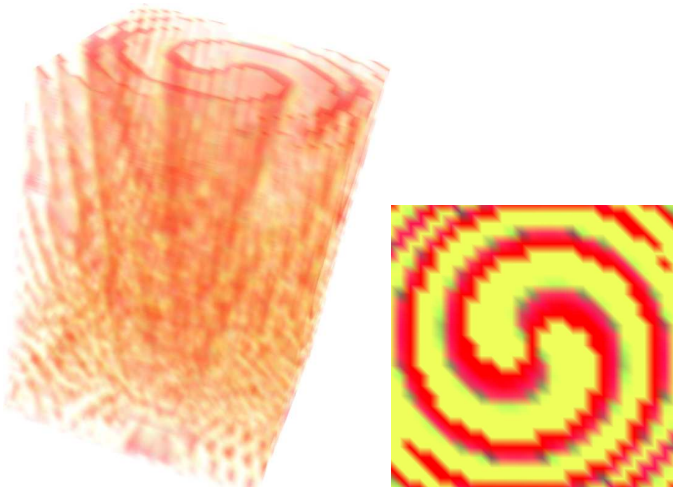

(a) (b)

Fig. 1: The rotational phase front of an OAM radio beam as obtained in our numerical simulations. The left–hand plot is a 3D visualization of the absolute phase of the electric fields. The right–hand plot depicts the plane which intersects the beam at $z = 50\lambda$ from the transmitting array. The rotational phase front of the OAM radio beam is clearly exhibited.

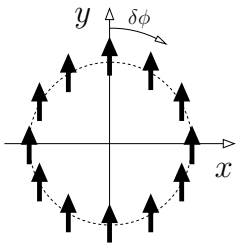

Fig. 2: Configuration of a typical OAM-generating antenna array used in the present work. In this case we used $N = 12$ electrically short dipoles, equidistantly spaced along the perimeter in a circular geometry, phased such that $\delta\phi = 2\pi l/N$.

the simulations, far-zone approximations of the fields must be avoided before the actual calculations are performed since, trivially,

$$\mathbf{J} = \int \varepsilon_0 \mathbf{r} \times \mathrm{Re}\{\mathbf{E}_{\mathrm{farzone}} \times \mathbf{B}^*_{\mathrm{farzone}}\}\, \mathrm{d}V = \mathbf{0}, \qquad (3)$$

showing that the OAM, transported to the far zone, is, in fact, produced by near and intermediate zone fields [14], [15]. This does not imply that the OAM of an EM field is restricted to the near or intermediate zone; on the contrary, as can be seen from Fig. 3, when in the near zone, pure angular momentum modes cannot be estimated reliably from Eq. (1), due to strong near-field **E** and **B** components. Since the OAM mode is defined by its rotating phase front, it is a highly phase dependent phenomenon and hence much smaller phase errors are tolerable than for an ordinary radiating system, where the standard tolerated far-field phase error is typically $\pi/8$ [16]. The rotating phase front created by the radiating antennas should be calculated as exactly as possible in order to achieve the necessary precision. Once the actual calculation is performed, one can adopt the far-zone approximation without losing information about the angular momentum mode.

We have produced our raw data (EM fields) by using the Maxwell equation solver NEC2 and the geometry editor of 4NEC2 [17]. However, our results are reproducible with any sufficiently accurate electromagnetic simulation tool. The calculations were performed in rectangular 3D volumes, sliced such that the z axis becomes the normal to the intersecting xy measurement planes. In each plane, the energy, Poynting flux, OAM, and the "spin" (*i.e.* wave polarization, SAM) are calculated from the 3D electric and magnetic fields. That the angular momentum can be calculated from intersecting planes was shown in [18].

IV. Directivity

The phase configuration of the OAM-generating circular array gives rise to coherent OAM-carrying radio beams with characteristic on-axis phase singularities and hence amplitude nulls at the centers of the beams.

In contrast to the highly collimated and cylindrical OAM laser beams [5], the spatial extent of the null region of the radio beams widens fast with the vertical distance to the transmitting array due to the conical beam intensity structure; see Fig. 3. Clearly, this makes it inappropriate to place the receiving antennas in the null at the center of the transmitted beam.

A convenient way to produce OAM modes is to use an array of electrically short dipoles. These small dipoles are geometrically simple and hence easier to work with in the simulation tool, but for practical purposes $\lambda/2$ dipoles may equally well be used. The basic configuration of the array of short dipoles can be seen in Fig. 2 for $N = 12$ elements.

Radiation patterns of four OAM modes generated with an antenna array with $N = 16$ elements are shown in Fig. 3. The width of the null along the z axis can be reduced with standard methods such as increasing the directivity of the individual elements, or widen the diameter of the circular array. Another way to generate more collimated OAM-carrying radio beams is to superimpose different OAM modes [6]; this technique will not be discussed in the present paper.

A. Number of elements of the array

The number of array elements has an additional influence on an OAM-generating antenna array compared to a regular antenna array: it determines how high l modes the array can generate. Theory predicts $-N/2 < l < N/2$ where N is the number of array elements [6].

In an ideal circular OAM dipole array, the short dipoles are continuously distributed along the circle. In the discrete approximation used here, OAM modes with too large values of l ($|l| \geq N/2$) will not generate a pure rotating phase front and hence no perfect OAM mode. The beam will be distorted and will not produce a stable OAM mode number over the whole conical intensity maximum profile.

The effect of a low number of antenna elements on the radiation pattern can be seen in Fig. 5, and its general effect on the gain maximum in the table next to it.

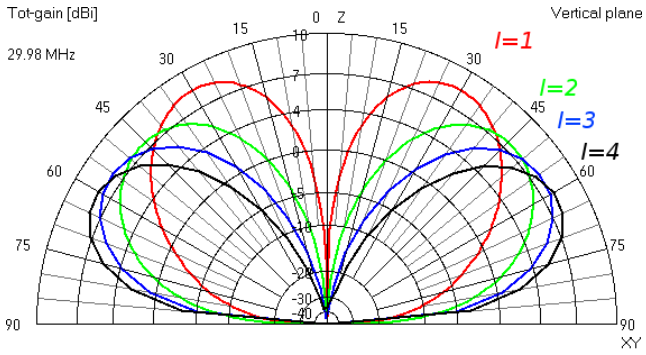

(a) Radiation pattern

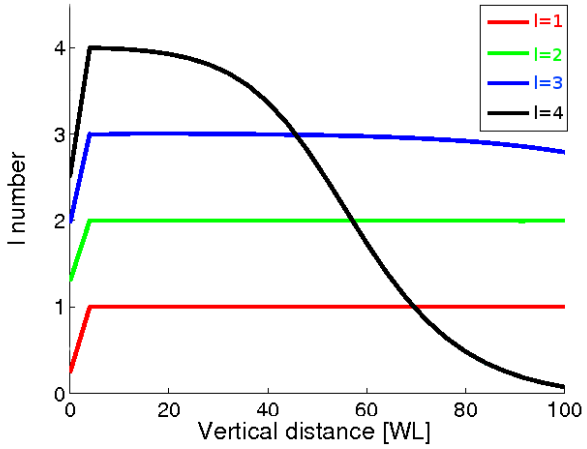

(b) OAM number wrt distance

Fig. 3: OAM beam profiles (a) for beams carrying OAM mode corresponding to $l = 1$ (red), $l = 2$ (green), $l = 3$ (blue) and $l = 4$ (black); and (b) the calculated behavior of the same beams as a function of distance from the antenna array. The fall-off for the higher l modes visible in (b) is due to the wide null in the simulation box (volume). The beam itself still carries the correct l mode but outside the simulation box. Due to low power density at the beam null, the simulation volume must be large enough to capture a part of the main beam. The beams were created with $N = 16$ electrically short dipoles placed in a circular array of diameter $D = \lambda$ and operating at a frequency of $f = 29.98$ MHz (10 m vacuum wavelength).

In fact, for practical purposes where the elements are not only short dipoles but, for instance, $\lambda/2$ dipoles, not even $l = N/2 - 1$ yields a satisfactory result. Then the measured OAM mode number will be close to the transmitted value but never quite reach it; see Fig. 4. It is reasonable to assume that these limiting cases are not as robust against noise as the other cases where one is far away from $N/2$, but this will be presented in a subsequent paper.

B. Aperture of the array

To minimize the null in the direction along the axis of the array, the diameter (aperture), D, of the circular array can be varied. We have studied a 12-element dipole array phased to create an $l = 1$ mode. By increasing the diameter of the array,

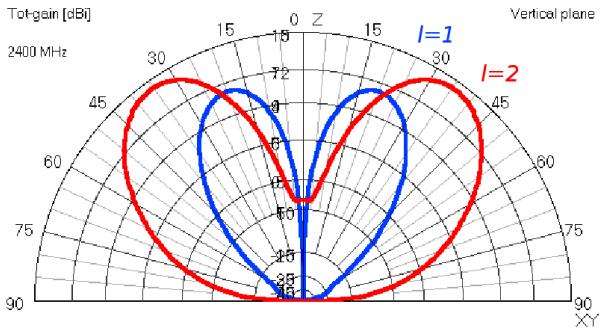

(a) Radiation pattern

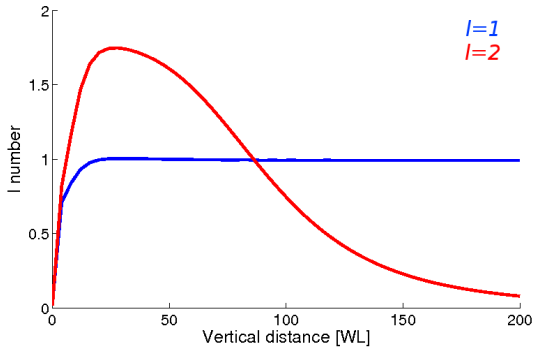

(b) OAM number wrt distance

Fig. 4: Generation of OAM modes with six $\lambda/2$ dipoles excited at 2.4 GHz in a circular array with $D = 1.5\lambda$. Here one observes the difficulty of being too close to the limit $|l| > N/2$ when one uses antennas, that are not electrically short. The array generates two modes, $l = 1$ (blue) and $l = 2$ (red), the radiation pattern is shown in panel (a) whereas the OAM mode number as a function of vertical distance to the array is shown in panel (b).

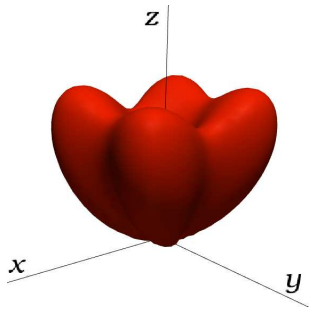

N	θ	$G^{\max}$ [dB]
4	32°	8.56
6	30°	8.44
7	30°	8.46
8	30°	8.49
9	30°	8.46
10	30°	8.52
11	30°	8.50
12	30°	8.48

Fig. 5: For a low number of elements in the circular array, such as the case $N = 4$ which is shown to the left, the radiation pattern exhibits ripples which vanish for $N \geq 6$. The table shows that the angle of maximum gain does not vary with the number of elements for an $l = 1$ OAM beam, when more than five antenna elements are used to generate the OAM-carrying beams. The diameter of the array is λ for all N, and the elements are excited at 29.98 MHz (10 m vacuum wavelength).

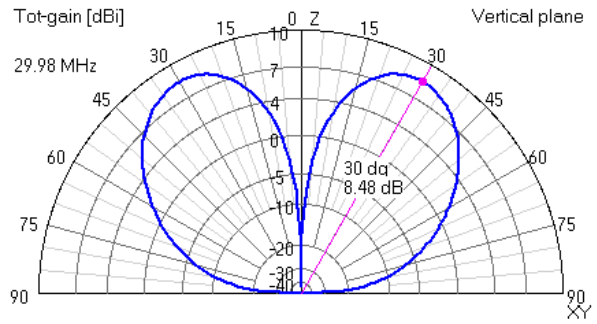

(a) $D = \lambda$

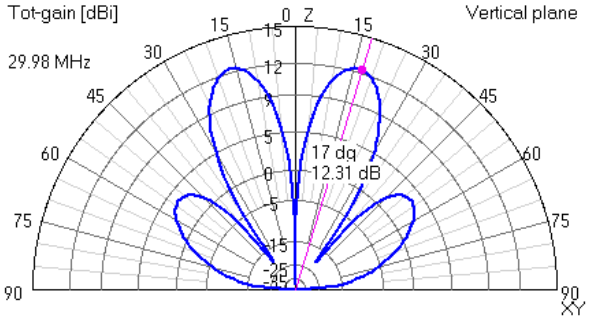

(b) $D = 2\lambda$

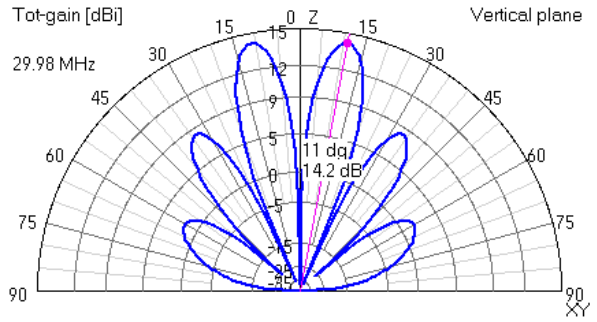

(c) $D = 3\lambda$

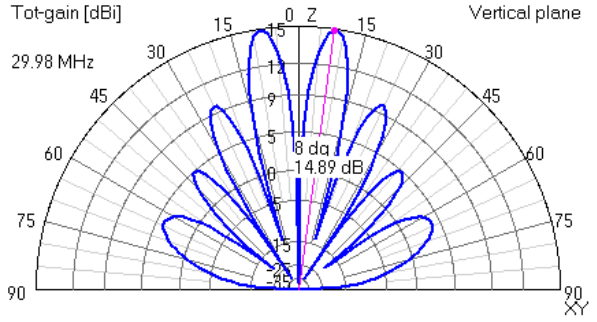

(d) $D = 4\lambda$

Fig. 6: Variation of the power density with the diameter D of the circular array for an $N = 12$ element array. When the diameter of the array is changed the pattern becomes more collimated and the side lobes increase. In all four cases, the beams carry the OAM mode number $l = 1$. The elements were operating at 29.98 MHz (10 m vacuum wavelength).

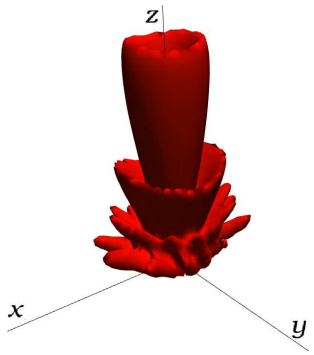

D [λ]	θ	$G^{\max}$ [dB]
0.5	41°	7.17
1.0	30°	8.48
1.5	21°	11.1
2.0	17°	12.31
2.5	13°	13.47
3.0	11°	14.2
3.5	10°	14.81
4.0	8°	14.89

Fig. 7: Plot (left) showing the 3D radiation intensity of a beam carrying OAM mode $l = 1$, generated by a circular array of $N = 12$ identical electrically short dipoles and with a diameter $D = 4\lambda$. Notice the almost cylindrical shape of the main lobe. The table (right) shows the variation of the angle θ of maximum gain, $G^{\max}$, when the diameter, D, of the circular array is varied. *cf.* Fig. 6d.

the angle of maximum gain is reduced, as seen in Fig. 6 and the table in Fig. 7. The radiation pattern in Fig. 7 illustrates the cylindrical shape of the beam for the case in Fig. 6d for a circle with $D = 4\lambda$.

The side lobes also increase with D. Because the side lobes are at much wider angles than the main lobe, they will not be detected by a narrow measurement along the beam axis and will have a small effect on the simulations; see Fig. 6. Of course, increasing side lobes mean a spatial dispersion of the energy, but for our OAM system simulation this has no significant importance.

V. Size of the Measurement Region

We shall now show that we do not need to measure the entire beam profile in order to get a reliable OAM measurement. It is, however, important to measure at the correct positions with respect to the beam axis.

A. Optimal measurement position

The OAM number l reflects the radiation intensity in a very direct way, as can be seen in Fig. 9. The asymmetries of the radiation pattern in Fig. 9b are reflected in the surface plot of the OAM mode number.

A measurement at the beam null will give a very weak signal and hence not a reliable OAM mode estimate, while a measurement in the major lobe will result in a strong signal and an accurate OAM mode estimate. In other words, when antenna arrays are used, a good OAM measurement position is more or less the same as a point of high beam intensity (Poynting vector or linear momentum intensity).

Any asymmetry of the radiation pattern will be reflected in the OAM mode measurement. The angular momentum intensity can be compared to the radiation intensity measurement by plotting the intensity of angular momentum, $|\mathbf{J}|$ together with the radiation intensity; this has been done in Fig. 8 for the case $l = 1$, $N = 12$, and $D = \lambda$. It can be seen that the angular momentum intensity has a more collimated structure than the

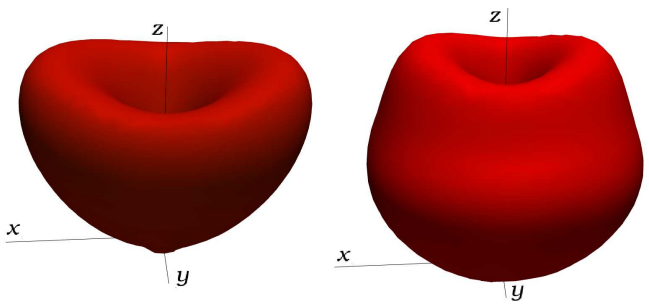

(a) 3D radiation intensity (b) 3D AM intensity

Fig. 8: Panel (a) shows the radiation intensity and (b) the angular momentum intensity for a radio beam carrying OAM proportional to $l = 1$. The beam nulls are along the z axes and the angular momentum intensity has a more collimated structure than the radiation intensity. In this case $N = 12$ and $D = \lambda$.

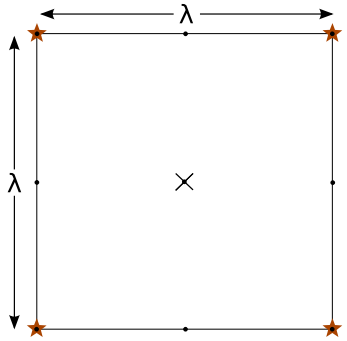

N	$l^{\text{meas}} - l^{\text{ideal}} [\times 10^{-3}]$
1^2	1.313
2^2	0.962
3^2	1.029
4^2	1.002
5^2	1.050
6^2	1.005
7^2	1.082
8^2	1.031
9^2	1.009
10^2	1.006

Fig. 10: The table displays how the deviation of the integrated OAM number from the ideal case, $l = 2$ depends on the number of grid points in the measurement area. The number of grid points have varied from 1^2 to 10^2 in discrete steps in a fix measurement area of size λ^2. The plot illustrates how the grid points where distributed for the first three calculations, 1^2 (cross), 2^2 (stars) and 3^2 (dots).

linear momentum one. That is, the boundary between the beam maximum and the beam null is sharper for the angular momentum intensity than for the radiation intensity. This makes us claim that the angular momentum intensity diagram is a better indication of where the angular momentum is measurable than the conventional radiation (linear momentum) intensity diagram.

B. Minimum measurement area

Another crucial question is over how large an area the fields must be measured for a fixed number of measurement points and an arbitrarily chosen fixed position in space. We have performed simulations for four fixed number measurement points, while we have varied the distance between the points from λ to $\lambda/10$. As can be seen in Fig. 9, the system does not exhibit any radical changes for different measurement areas. The only substantial variations of the OAM number occur in the beam null, where there in any case is no usable signal. Fig. 9c shows that even though there is a slight measurement improvement when one uses larger measurement cross sections, they are still within 10% of the desired (created) OAM number (in this case $l = 2$).

C. Minimum number of measurement points

Another important question is how many measurement points are needed within a fixed area in order to measure an OAM mode integer within $l^{\text{ideal}} \pm \varepsilon$, where ε is the measurement error of the desired OAM number l^{ideal}. As can be seen in the table in Fig. 10, the number of points can be rather small without affecting the OAM mode number.

From a field perspective, if the 3D electric and magnetic fields are measured and the position of the beam axis is known (or the exact position and orientation of the source is known), the OAM mode number is a locally measurable quantity, *i.e.*, can be measured in a small surrounding of a single point. This result may appear surprising because in laser experiments the entire beam profile is usually measured in order to estimate the OAM mode number [4]. Nevertheless, the OAM of an electromagnetic beam is as much a property of the fields themselves [19] as is the polarization or the Poynting flux, and this suggests that it should be as stable or unstable as the other electromagnetic quantities.

D. OAM and polarization

So far we have not taken into account the polarization of the field, *i.e.*, the spin angular momentum, SAM, which is a frequently utilized rotational/topological quantity in radio science and applications. Can the two different rotational modes, OAM and SAM, be distinguished and, if so, how? In fact, SAM (polarization) modes and OAM modes can be separated. Instead of using a circular array of dipoles to generate $l = 1$, an array of crossed dipoles may be used to generate a perfect circularly polarized field with the same l but also with an additional SAM mode number s.

If one only considers $\mathbf{J}$, some of the modes will become degenerate. Consider for instance two different beams, one carrying OAM $l = 1$ and SAM $s = -1$, and a second beam carrying OAM $l = -1$ and SAM $s = 1$, as seen in Fig. 11. In both cases the total angular momentum mode number $j = l + s = 0$. The AM mode number j cannot be separated into l and s without separately determining s by either calculating the polarization from the generalized Stokes parameter $\mathbf{V}$ [11], [12], [13] or by separating the signal by only measuring the vertical or horizontal polarization.

In order to determine the polarization from the generalized Stokes parameters, we consider the z component of the 3D Stokes parameter [11], [12], [13]

$$V_z = \{\mathbf{V}\}_z = -\frac{\varepsilon_0}{2} \operatorname{Im}\left\{\mathbf{E} \times \mathbf{E}^* + c^2 \mathbf{B} \times \mathbf{B}^*\right\}_z \tag{4}$$

which can be normalized such that

$$\frac{\int V_z \mathrm{d}V}{\frac{\varepsilon_0}{2} \int (|\mathbf{E}|^2 + c^2 |\mathbf{B}|^2) \mathrm{d}V} = \pm 1 \tag{5}$$

which, for the special case of a circular polarized beam, equals s.

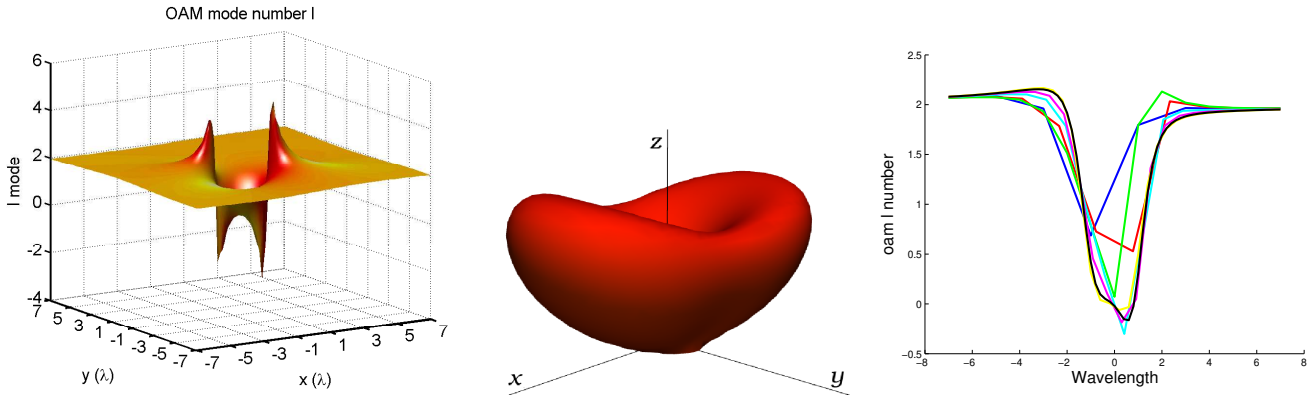

(a) (b) (c)

Fig. 9: OAM measurement simulations for a beam carrying OAM mode number $l = 2$, generated by 12 short electric dipoles in a circular array with diameter $D = \lambda$. Panel (a) shows l estimated in a plane 50λ away from the circular array and perpendicular to the z axis, *i.e.*, the beam axis. Panel (b) shows the 3D radiation intensity. Here each OAM number is averaged over four grid points, which in panel (a) are separated by 0.1λ. This means that the measurement area is only $0.01\lambda^2$. Panel (c) shows the dependence of the calculated OAM mode number on the position of the measurement area when the position is passing from the beam maximum through the beam null and to the beam maximum on the other side of the null. The colors correspond to the side of the measurement square, *i.e.*, the distance between two adjacent measurement points, as follows: blue, 1.00λ, red, 0.75λ green, 0.50λ cyan, 0.40λ magenta, 0.30λ yellow, 0.20λ and black 0.10λ. The asymmetries in the radiation intensity are directly reflected in the measurement of the OAM mode number. At positions where the field is weak, *e.g.* in the beam null, the OAM mode number deviates significantly from $l = 2$.

VI. Conclusions and Discussion

We have demonstrated that the basic behavior of an OAM antenna system is similar to most other conventional antenna systems. Hence, the directivity properties *etc.* can be enhanced by standard methods and we can use existing optimization methods to utilize OAM in radio beams.

We have also demonstrated that only a local measurement is needed in order to detect OAM in a radio beam, provided that the location of the beam axis is known. In our simulations, neither the number of measurement points nor the measurement area affect significantly the (noiseless) measured OAM mode of the field.

In the optics literature dealing with OAM [20], it is shown that paraxial Laguerre–Gauss (LG) modes carry OAM and therefore have non–planar, rotating (helical) phase fronts. Although the OAM antenna array system does not generate pure LG beams, a rotation in the phase front is clearly visible even in radio beams which carries OAM; see Fig. 1. This suggests that the radio beams, generated in this way have similarities with L-G beams.

Acknowledgment

We gratefully acknowledge the financial support from the Swedish Research Council (VR), Swedish Governmental Agency for Innovation Systems (VINNOVA) and the Swedish Space Board (SNSB). We also thank Leif Gustafsson for useful comments and discussions.

References

[1] J. D. Jackson, *Classical Electrodynamics*, 3rd ed. New York: Wiley, 1998, ch. 7, Problem 7.29.

[2] J. Schwinger, L. L. DeRaad, Jr., K. A. Milton, and W. Tsai, *Classical Electrodynamics*. Reading, MA: Perseus Books, 1998.

[3] R. A. Beth, "Mechanical detection and measurement of the angular momentum of light," *Phys. Rev.*, vol. 50, no. 2, pp. 115–125, 1936.

[4] G. Gibson, J. Courtial, M. J. Padgett, M. Vasnetsov, V. Pas'ko, S. M. Barnett, and S. Franke-Arnold, "Free-space information transfer using light beams carrying orbital angular momentum," *Opt. Express*, vol. 12, no. 25, pp. 5448–5456, 21 November 2004.

[5] L. Allen, M. W. Beijersbergen, R. J. C. Spreeuw, and J. P. Woerdman, "Optical angular momentum of light and the transformation of Laguerre-Gauss laser modes," *Phys. Rev. A*, vol. 45, pp. 8185–8189, 1992.

[6] B. Thidé, H. Then, J. Sjöholm, K. Palmer, J. E. S. Bergman, T. D. Carozzi, Y. N. Istomin, N. H. Ibragimov, and R. Khamitova, "Utilization of photon orbital angular momentum in the low-frequency radio domain," *Phys. Rev. Lett.*, vol. 99, no. 8, p. 087701, 22 August 2007.

[7] G. Turnbull, D. A. Robertson, G. M. Smith, L. Allen, and M. J. Padgett, "The generation of free-space Laguerre-Gaussian modes at millimetre wave frequencies by use of a spiral phaseplate," *Optics Communications*, vol. 127, pp. 183–188, 1996.

[8] S. M. Barnett, "Optical angular-momentum flux," *J. Opt. B: Quant. Semiclass. Opt.*, vol. 4, pp. S7–S16, 2002.

[9] J. Humblet, "Sur le moment d'impulsion d'une onde électromagnétique," *Physica*, vol. X, no. 7, pp. 585–603, 1943.

[10] J. Courtial, D. A. Robertson, K. Dholakia, L. Allen, and M. J. Padgett, "Rotational frequency shift of a light beam," *Phys. Rev. Lett.*, vol. 81, no. 22, pp. 4828–4830, 1998.

[11] T. Carozzi, R. L. Karlsson, and J. Bergman, "Parameters characterizing electromagnetic wave polarization," *Phys. Rev. E*, vol. 61, pp. 2024–2028, 2000.

[12] J. E. S. Bergman, S. M. Mohammadi, T. D. Carozzi, L. K. S. Daldorff, B. Thidé, R. L. Karlsson, and M. Eriksson, "Conservation laws in generalized Riemann-Silberstein electrodynamics," *arXiv*, vol. 0803.2383, 2008. [Online]. Available: http://arxiv.org/abs/0803.2383

[13] C. Brosseau, *Fundamentals of Polarized Light: A Statistical Optics Approach*. New York: Wiley, 1998.

[14] V. M. Abraham, "Der Drehimpuls des Lichtes," *Physik. Zeitschr.*, vol. XV, pp. 914–918, 1914.

[15] B. Thidé, *Electromagnetic Field Theory*. Uppsala, Sweden: Upsilon Books, September 2007, on-line Internet version: http://www.plasma.uu.se/CED/Book.

[16] C. A. Balanis, *Antenna Theory*, 3rd ed. New York: John Wiley and Sons, 2005.

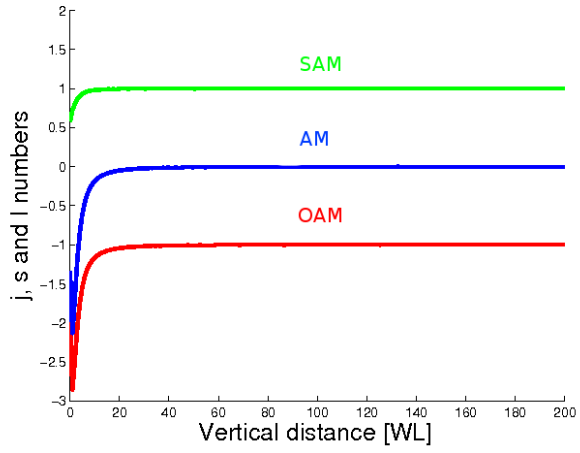

(a) $l = 1$, $s = -1$

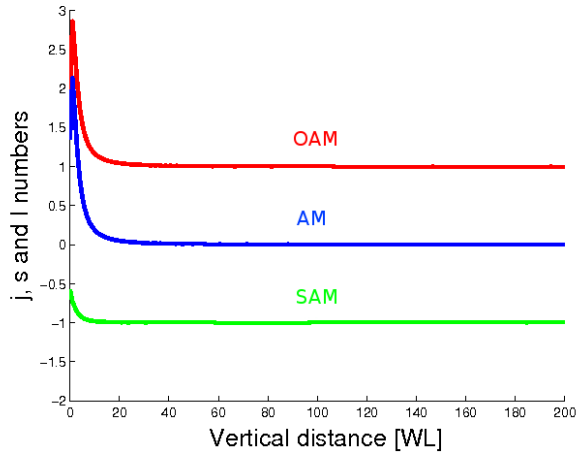

(b) $l = -1$, $s = 1$

Fig. 11: Two different beams, corresponding to two degenerate cases of angular momentum mode number $j = 0$ when (a) OAM mode number $l = 1$, SAM mode number $s = -1$ and (b) $l = -1$, $s = 1$. If only the angular momentum $\mathbf{J} = \int \varepsilon_0 \mathbf{r} \times \mathrm{Re}\{\mathbf{E} \times \mathbf{B}^*\} \mathrm{d}V$ is measured, the two cases are indistinguishable. However, they can be resolved if the generalized Stokes parameter $\mathbf{V}$ is used to determine s.

[17] A. Voors, "4NEC2." [Online]. Available: http://home.ict.nl/~ arivoors/
[18] M. V. Berry, "Paraxial beams of spinning light," in *Singular Optics*, M. S. Soskin, Ed., vol. 3487, The International Society for Optical Engineering. SPIE, August 1998, pp. 6–11.
[19] A. Mair, A. Vaziri, G. Weihs, and A. Zeilinger, "Entanglement of the orbital angular momentum states of photons," *Nature*, vol. 412, pp. 313–316, 2001.
[20] L. Allen, S. M. Barnett, and M. J. Padgett, *Optical Angular Momentum*. Bristol, UK: IOP, 2003.